Journal of Catalysis **211,** 285–295 (2002)
doi:10.1006/jcat.2002.3684

Synthesis of Methanethiol from Methanol over Reduced Molybdenum Sulfide Catalysts Based on the Mo_6S_8 Cluster

Thomas J. Paskach,*,‡ Glenn L. Schrader,*,‡,[1] and Robert E. McCarley†,‡

*Department of Chemical Engineering; †Department of Chemistry; and ‡Ames Laboratory–USDOE, Iowa State University, Ames, Iowa 50011

Received November 21, 2001; revised May 10, 2002; accepted May 21, 2002

Catalysts having structures containing the Mo_6S_8 cluster (crystalline Chevrel phases, amorphous ternary molybdenum sulfides, and ligated molecular clusters) have been discovered to be active for thiol synthesis from methanol and hydrogen sulfide at 250°C and 1 atm. An amorphous lanthanum molybdenum sulfide material was found to be the most selective catalyst (>80% methanethiol) at low conversions. CO_2, CO, CS_2, and CH_4 were the major by-products in these studies. © 2002 Elsevier Science (USA)

Key Words: **methanethiol synthesis; organosulfur catalysis; molybdenum sulfide cluster catalysts.**

INTRODUCTION

Industrial synthesis of bulk organosulfur chemicals includes the production of mercaptans (thiols), alkylsulfides (thioethers), polysulfides, and thiophenes. Many of the derivatives of these organosulfur chemicals have biological activity and are used extensively in the production of agrochemicals and pharmaceuticals. Low-molecular-weight mercaptans such as C_1–C_6 thiols are commercially manufactured on the order of 10^4 ton/year. For example, methanethiol (MeSH) is used for the production of methionine (an important poultry feed supplement) and methanesulfonyl chloride. Other mercaptans, especially higher molecular weight compounds, are used in the manufacture of rubber and plastics and in the production of polysulfides for lubricant additives. However, excessive amounts of some alkylsulfide by-products are also produced, which necessitates reprocessing or incineration.

Both surface-catalyzed and free-radical processing routes are used industrially for mercaptan manufacture, and significant claims for catalytic selectivity have been discussed in the patent literature, with examples of selectivity to MeSH of nearly 100% (1–4). Metal oxide catalysts are used for the production of MeSH from methanol (MeOH) and H_2S, including (i) KOH-promoted commercial hydrodesulfurization (HDS) catalysts, which consist of sulfided Ni–Mo, Ni–W, Co–Mo, or Co–W oxides supported on alumina (5), (ii) sulfided α- or β-alumina trihydrate on KOH-treated γ-Al_2O_3 (6, 7), (iii) K_2WO_4 on alumina promoted with KOH, and (iv) KOH on alumina (8). Major side products are typically dimethylsulfide (DMS), dimethylether (DME), and methane. Use of secondary alcohol feeds results in formation of olefins via dehydration. Solid acid catalysts such as dry cation-exchange resins are used in mercaptan synthesis from alcohols or olefins and H_2S; however, they may deactivate with alcohols due to the formation of water. These catalysts can be very selective for the production of secondary or tertiary thiols from olefins. For α-olefins, the reaction follows Markownikoff addition of SH^- to the double bond. Free-radical synthesis is used for production of primary mercaptans from α-olefins and H_2S (anti-Markownikov addition). Conversion assisted by UV radiation is fairly selective to the primary mercaptan (~92% selectivity), and homogeneous catalysts containing boron (9), which apparently generate radicals, can be even more selective (up to ~97%).

The carbon oxides have been studied as feedstocks for production of MeSH (10), starting with synthesis gas (CO and H_2) or a mixture of CO_2 and H_2. Sulfur sources were either H_2S or elemental sulfur, and catalysts for these processes were W–K/Al_2O_3 (11) and various other metal oxides (Cr, Ni, Zn).

In our recent research, a new family of materials based on the Mo_6S_8 molecular structure (Fig. 1) has been shown to be effective catalysts for MeSH synthesis from MeOH and H_2S. The categories of materials examined in this work were (i) crystalline Chevrel phases, $M Mo_6S_8$, where M is a ternary metal such as La; (ii) amorphous ternary molybdenum sulfides, $M_x^{+n}(Mo_6S_8)S_{xn/2}$, where M is a ternary metal such as La, Ho, Sn, Pt, or Na; (iii) amorphous or crystalline molecular cluster materials, $(Mo_6S_8)L_y$, where L is a ligand such as piperidine (pip) or propylamine ($PrNH_2$); and (iv) an amorphous, ligated, ternary material with the formula $Na_{2x}(Mo_6S_8)S_x(py)_y$ [NaMoS(py)], where py refers to a pyridine ligand (12). Crystalline Chevrel phases and various amorphous ternary molybdenum sulfides such as LaMoS have been studied previously in our research and

[1] To whom correspondence should be addressed. E-mail: schrader@iastate.edu.

0021-9517/02 $35.00

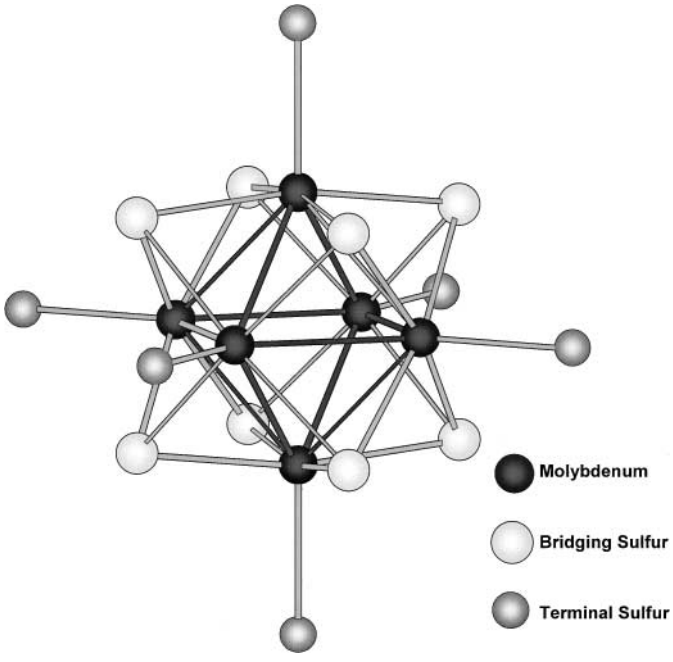

FIG. 1. Structure of the Mo_6S_8 hexanuclear cluster unit which is formed by a molybdenum octahedron and eight triply bridging sulfur atoms capping each face. Additionally, six terminal positions are located at the vertices of the octahedron and are occupied by either organic ligands or sulfur atoms.

have been found to be active and stable HDS catalysts. In this paper, we provide the first report of the catalytic properties of these Mo_6S_8 cluster materials for thiol synthesis.

EXPERIMENTAL

Catalyst Synthesis

Preparations for the various reduced molybdenum sulfides used in this research have been reported previously (13–16). Amorphous ternary materials (Samples a, b, c, and d in Tables 1 and 2) were prepared by a two-step process. In the first step, anhydrous Mo_6Cl_{12} reacted with sodium hydrosulfide (NaSH) and sodium butoxide (NaOBu) under refluxing anhydrous *n*-butanol (BuOH) to form a black, amorphous sodium salt containing either two or three Na atoms per cluster. The solid $Na_{2x}(Mo_6S_8)S_x$ (Sample e, Tables 1 and 2, and also referred to as NaMoS) was filtered and washed with anhydrous, degassed MeOH to remove NaCl.

$$Mo_6Cl_{12} + (8+x)NaSH + (4+x)NaOBu \xrightarrow{BuOH} Na_{2x}(Mo_6S_8)S_x + (4+x)BuOH + 12NaCl \quad [1]$$

In the second step, NaMoS was treated with a metal salt [for example, $La(NO_3)_3 \cdot 6H_2O$] in anhydrous, degassed MeOH, so ion exchange occurred between the metal atoms and the Na ions to form the amorphous ternary molybdenum sulfide (also referred to as LaMoS).

$$Na_3(Mo_6S_8)S_{1.5} + La^{3+} \xrightarrow{MeOH} La(Mo_6S_8)S_{1.5} \cdot y(MeOH) + 3Na^+ \quad [2]$$

A partially ligated material, NaMoS(py) [Sample f, Tables 1 and 2], was prepared by adding pyridine to the mixture at the start of Reaction 1:

$$Mo_6Cl_{12} + (8+x)NaSH + (4+x)NaOBu \xrightarrow[\text{pyridine}]{BuOH} Na_{2x}(Mo_6S_8)S_x(py)_y + (4+x)BuOH + 12NaCl. \quad [3]$$

Crystalline, fully ligated clusters, from which Samples h and i in Tables 1 and 2 were derived, were prepared by refluxing the liquid ligand in an extractor over the solid NaMoS(py). In each case, the fully ligated cluster was soluble in excess ligand and so was the only product found in the extract (12):

$$2nNa_{2x}(Mo_6S_8)S_x(py)_y(MeOH) \xrightarrow{Ligand} nNa_{4x}(Mo_6S_8)S_{2x}(py)_{6(solid)} + n(Mo_6S_8)L_{6(soln)}. \quad [4]$$

The crystalline Chevrel phase $LaMo_6S_8$ (Sample g, Tables 1 and 2) was prepared from La, Mo, and S in a molar ratio of 1 : 6 : 8 by performing two annealing/grinding cycles in sealed fused silica tubes sealed under dynamic vacuum. The material was heated for 2 days at 1100–1150°C during each cycle. Powder X-ray diffraction confirmed that the material was virtually pure $LaMo_6S_8$ Chevrel phase, though some weak peaks characteristic of Mo_2S_3 were observed.

TABLE 1

Activity and Surface Areas of Various Amorphous Catalysts Containing the Mo_6S_8 Cluster Unit, at 250°C, with H_2S/MeOH Ratio of 3

Label	BET surface area (m^2/g)		MeOH conversion		
	Prereaction	Postreaction	μmol/ h · g_{cat}	μmol/ h · m^2	mol%
a $La(Mo_6S_8)S_{1.5}$	170	116	1360	12	10.2
b $Ho(Mo_6S_8)S_{1.5}$	176	14	2031	147	15.2
c $Sn(Mo_6S_8)S$	130	18	375	21	2.9
d $Pt(Mo_6S_8)S$	130	28	523	18	3.9
e $Na_3(Mo_6S_8)S_{1.5}$	135	46	1425	31	10.7
f $Na_2(Mo_6S_8)S(py)_y$	138	38	806	21	6.0
g $LaMo_6S_8$	0.46	0.47	84	178	1.2
h $Mo_6S_8(pip)_y$	0.80	1.47	623	424	4.7
i $Mo_6S_8(PrNH_2)_y$	0.83	0.41	131	317	1.4
j MoS_2	10	8.7	334	38	2.5

Note. Data represents the average for the final 2 h of a 20-h run.

TABLE 2

Selectivity of the Various Amorphous Catalysts to the Major Products of the Reaction of H_2S and MeOH at 250°C and H_2S/MeOH Ratio of 3

Label	Selectivities (mol% equivalent)								
	MeSH	DMS	DME	CH_4	CO	CO_2	COS	CS_2	Other products
a $La(Mo_6S_8)S_{1.5}$	83.0	6.4	0.1	0.1	5.0	2.6	0.2	2.5	0.1
b $Ho(Mo_6S_8)S_{1.5}$	72.2	17.4	0.9	0.4	2.6	2.7	0.1	3.4	0.1
c $Sn(Mo_6S_8)S$	75.0	11.0	2.7	0.6	8.2	2.5	0.0	0.0	0.0
d $Pt(Mo_6S_8)S$	75.4	8.0	0.7	0.9	5.5	0.4	1.0	8.1	0.0
e $Na_3(Mo_6S_8)S_{1.5}$	44.9	0.1	0.0	0.2	13.6	18.3	19.0	3.9	0.0
f $Na_2(Mo_6S_8)S(py)_y$	51.9	0.3	0.0	0.2	11.9	11.3	15.5	8.9	0.0
g $LaMo_6S_8$	53.6	0.0	0.6	0.1	38.1	6.5	1.0	0.0	0.0
h $Mo_6S_8(pip)_y$	59.9	4.7	0.1	0.6	16.2	0.0	4.9	13.7	0.1
i $Mo_6S_8(PrNH_2)_y$	20.8	0.0	0.1	1.1	65.3	5.2	0.8	5.0	1.7
j MoS_2	36.5	4.6	8.1	0.0	50.7	0.0	0.0	0.0	0.1

Note. Data represents the average for the final 2 h of a 20-h run.

Mo_6S_8-based catalysts have generally been found to be oxygen sensitive. Schlenk techniques with a high vacuum line and a Vacuum Atmospheres Company model 8130 drybox with oxygen and moisture gettering capabilities were utilized.

Catalyst Characterization

Catalyst characterization involved infrared spectroscopy (FTIR), laser Raman spectroscopy (LRS), X-ray photoelectron spectroscopy (XPS), and adsorption surface area/pore size measurements.

FTIR spectra were obtained using a Bomem MB-102 spectrometer with CsI optics, at 2-cm^{-1} resolution. Samples were analyzed as mineral oil mulls with special sample holders designed to exclude O_2.

LRS was performed using a Coherent 532-50 diode-pumped solid-state laser (532-nm, 50-mW source) with fiber optic couplings and integral source/collection optics. Spectra were taken in a backscattered collection mode and consisted of the summation of three scans of 60 s each. A Kaiser Holospec f/1.8 spectrometer and Princeton Instruments CCD detector (1100×330 yielding 1.2 cm^{-1}/pixel resolution) with WinSpec software were used for signal analysis. Catalyst samples were analyzed in capillary tubes or the Pyrex reactor tubes for postreaction LRS characterization due to their oxygen sensitivity.

XPS data were obtained with a Physical Electronics Industries 5500 multitechnique surface analysis system using a monochromatic Mg$K\alpha$ source; binding energies were calibrated with adventitious carbon (C 1s = 284.6 eV). Spectra were fit with peaks consisting of a mixture of Lorentzian and Gaussian character, following Shirley background subtraction. For doublet peak fitting, the peak area ratios and doublet offset value were fixed. Air contamination was avoided in the XPS measurements by using a special airtight sample holder that was loaded in the drybox and opened in the airlock sample port of the XPS instrument, under vacuum.

Surface areas were measured with a Micromeretics ASAP 2010C instrument at 77 K. N_2 was used as the adsorbate for amorphous materials whereas Kr was used as the adsorbate for crystalline materials. Brunauer, Emmet, and Teller (BET) calculations were used to determine surface areas for all samples, and the Barret, Johner, and Hallenda (BJH) method was used for determining pore size distributions for the amorphous samples. Samples were degassed overnight at 150°C under dynamic vacuum prior to analysis.

Catalytic Reactor Studies

H_2S (VLSI grade) was supplied by Scott Specialty Gases. Certified MeOH (Fisher) was degassed in the saturator with bubbling He prior to use. UHP (zero) He (Matheson) was used for the GC carrier and as a reactor feed or product diluent.

The microreactor system (Fig. 2) used 200–400 mg of catalyst fixed in a 6-mm O.D. × 4-mm I.D. Pyrex reactor tube.

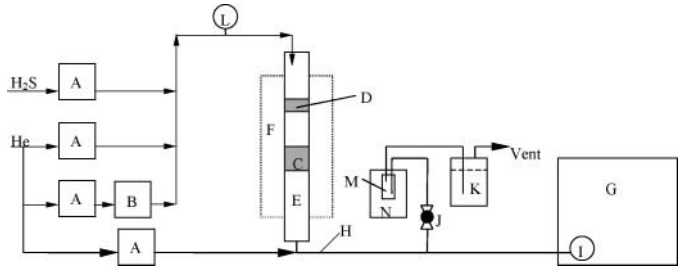

FIG. 2. Microreactor system. A, Mass flow controllers; B, saturator for MeOH feed; C, catalyst bed with quartz wool plugs on top and bottom; D, quartz wool plug for liquid feed evaporator; E, Pyrex or quartz tube reactor; F, temperature-controlled reactor furnace; G, GC with FID and TCD; H, heat tracing; I, sample injection valve; J, split valve; K, KOH/bleach bubbler; L, pressure gauge; M, trapping vial; N, ice–salt bath.

A 4-mm O.D. × 2-mm I.D. Pyrex tube was inserted in the lower half of the larger tube for catalyst bed support. Small (2–3 mm) plugs of silane-treated quartz wool held the catalyst bed in place. Since the catalyst was air sensitive, the reactor tube was fitted on both ends with Swagelock fittings with high-temperature rubber septa and loaded in the drybox. Installation of the reactor involved piercing the septa with needles under a He purge. The temperature in the reactors was maintained with a Lindberg model 54032 furnace with an Omega 4200 or Eurotherm 815P programmable temperature controller.

Gas feeds were controlled with Brooks model 5850 and 5850E mass flow controllers and model 5878 master controller. MeOH was delivered by saturating a He flow at a controlled temperature with the feed liquid. He was added to the reactor effluent line to dilute the reactor effluent and to prevent condensation. Pressure (approximately 1 atm) was controlled in the reactor by use of a needle valve on the reactor outlet located downstream of the He addition, which split the flow between the sample loop and the vent/scrubber system.

Product analysis was performed with a Varian model 3600CX gas chromatograph (GC) with a flame ionization detector (FID) and thermal conductivity detector (TCD) in parallel. An Alltech AT-SULFUR (30 m × 0.32 mm, 4-μm film thickness) column was used with a 5 m × 0.32 mm deactivated fused silica guard column. The GC was programmed from 50°C (5 min) to 150°C at 10°C/min and then to 250°C at 20°C/min. All lines from the reactor were also heated electrically over the 150–200°C range using Omega 6100 thermostats to prevent product condensation.

GC peaks were identified by trapping products in an amber septum vial in an ice–salt bath, with subsequent analysis by a Finnigan TSQ 700 GC–mass spectrometer system having both electron impact ionization and ammonia positive ion impact ionization modes. The first quadrupole was used as the analyzer and was scanned from m/z 35 to 400 at a rate of 0.5 s per scan. The second and third quadrupoles were maintained in at RF-only mode. Unit mass resolution was achieved using FC43 as the calibration and tuning reference. GC retention times were also compared with known standards.

TCD molar response factors were measured with known standards for CO, CO_2, and CS_2. The TCD response factor for COS was assumed to be the same as for CO_2. FID molar response factors were measured for MeOH and estimated for the remaining products using the methods reported by Ackman (17, 18).

RESULTS

Reaction Studies: Activity and Selectivity Comparisons

The activity and selectivity of various catalysts containing the Mo_6S_8 cluster were compared for MeSH synthesis from MeOH and H_2S. For all the experiments in the comparison studies, the feed rate of MeOH was 1.00 sccm, and the H_2S rate was 3.00 sccm (H_2S/MeOH ratio of 3). Reactions were carried out for 20 h at 250°C, and average activities and selectivities for the last 2 h are reported in Tables 1 and 2. Reaction products were MeSH, DMS, DME, CS_2, CH_4, CO, CO_2, and COS, but trace amounts of other products (H_2, ethane, and ethene) were also detected.

All the materials listed in Tables 1 and 2 were active catalysts. However, the various Mo_6S_8 materials ranged widely in their specific activities (expressed as the rate of MeOH converted per unit of catalyst weight or per unit surface area after reaction) and selectivities to MeSH and the major by-products (DMS, CO, CO_2, CS_2, and COS). Activities ranged from 12 to over 400 μmol/h · m^2, and selectivities to MeSH ranged from 21 to 83%.

For the amorphous ternary materials, MeSH selectivity depended on the ternary metal. It is interesting that amorphous LaMoS had the lowest specific activity but also the highest selectivity for MeSH. Amorphous HoMoS had the highest activity of all the amorphous materials, both on a weight and on a surface area basis; however, its selectivity to MeSH was slightly lower, at about 72%. Both Ho and La are both considered large ions in the Mo_6S_8 system. Ternary materials containing Na had relatively low selectivity for MeSH and much higher selectivity for COS, CO_x, and CS_2.

If activities were compared based on rates expressed on a surface area basis (mol/m^2 · s), catalysts with lower surface areas apparently tended to be superior. For example, although the Chevrel material $LaMo_6S_8$ had activity on a per-weight basis more than an order of magnitude lower than that of amorphous LaMoS, the specific activity on a per-surface-area basis was more than an order of magnitude higher.

Effect of H_2S/MeOH Ratio

The effect of the H_2S/MeOH ratio on activities and selectivities was examined using amorphous LaMoS (Table 3). For these studies, the reactor temperature was maintained at 250°C. As the feed rates of MeOH and/or H_2S were changed, He makeup was added to the reactor inlet to maintain a total reactor gas feed rate of 15 sccm. The catalyst was stabilized for 72 h prior to data collection. The selectivity toward DMS and CO_2 increased noticeably as the H_2S/MeOH ratio was decreased. However, as the H_2S/MeOH ratio was increased, the selectivity toward CS_2 increased steadily. The result of these two combined effects was that the selectivity toward MeSH was much more constant over nearly the entire range of H_2S/MeOH studied. There was a slight maximum, however, at about 3, and the selectivity to MeSH did not drop appreciably until the H_2S/MeOH ratio was significantly below the stoichiometric value of 1 (Table 3). Also of note was the fact that even

TABLE 3

Conversion and Selectivities for Amorphous LaMoS at 250°C Reaction Temperature, at Various Values of H_2S/MeOH Ratio

H_2S/MeOH (mol/mol)	MeOH conversion (mol%)	Selectivities (mol%)							
		MeSH	DMS	DME	CH_4	CO	CO_2	COS	CS_2
0.30	19.5	60.0	11.6	0.16	0.59	6.4	15.1	0.1	6
0.50	16.9	68.5	7.2	0.16	0.38	6.3	13.6	0.3	3
1.00	15.3	71.1	4.3	0.14	0.27	6.3	11.4	0.5	6
2.00	13.3	72.0	2.6	0.10	0.20	5.5	9.9	0.6	9
3.00	12.0	72.3	1.9	0.10	0.17	5.3	8.1	0.6	11
4.00	11.1	71.7	1.5	0.06	0.14	4.4	7.4	0.9	14
6.00	10.1	71.4	1.2	0.04	0.12	5.4	6.7	1.2	14

though H_2S was a reactant, the conversion of MeSH formation decreased with increasing H_2S/MeOH ratios; i.e., excess H_2S tended to suppress the reaction for the values of H_2S partial pressure examined.

Catalyst Stability

Characterization by LRS and FTIR was performed to examine the stability of the Mo_6S_8 cluster. The far-IR spectrum of materials incorporating the Mo_6S_8 cluster includes a band at around 385 cm^{-1} arising from the Mo–S stretching vibration; occasionally a weaker band at about 253 cm^{-1} arising from Mo–Mo bond vibrations can also be observed (12). Amorphous materials containing the Mo_6S_8 cluster show essentially no Raman bands, while crystalline molecular compounds and other crystalline phases with the Mo_6S_8 cluster may show one sharp band at about 408–411 cm^{-1} (12). Crystalline (and also to some degree poorly crystalline) MoS_2 is expected to give rise to sharp IR bands at about 385 and 470 cm^{-1} and sharp Raman bands at about 384 and 408 cm^{-1} (19, 20). Therefore, detection of IR bands at 470 cm^{-1} or Raman bands at both 384 and 408 cm^{-1} indicates the presence of MoS_2. For both of these characterization methods, spectra taken of mechanical mixtures made with fresh catalyst and pure MoS_2 indicated that the detection limit for MoS_2 was less than 10%.

LRS characterization (Fig. 3) after reaction showed that ternary materials involving Sn, Pt, and Na partially converted to MoS_2 after 20 h at 250°C. However, La and Ho ternary materials did not appear to form MoS_2, nor did the ligated crystalline molecular clusters. LRS is particularly sensitive to these species: spectra of mechanical mixtures of 10% MoS_2 in fresh catalysts clearly revealed the large peaks at 383 and 404 cm^{-1}.

All the amorphous catalysts lost a significant fraction of their surface area under reaction conditions. Crystalline materials did not show much change in surface area, except that the piperidine-ligated crystalline molecular cluster actually showed a significant increase in surface area under reaction conditions.

Expanded Studies of LaMoS and NaMoS(py)

To examine the stability characteristics in greater detail with respect to time and temperature, several additional reactor studies were carried out with amorphous LaMoS and NaMoS(py). These stability studies were conducted for 72 h at 250, 300, and 350°C, with subsequent characterization by LRS, FTIR, XPS, and adsorption measurements. For these stability studies, 200 mg of catalyst was used, and the H_2S/MeOH ratio was 3. Catalyst contact times based on the feed composition at reactor conditions were on the order of 1 s (Table 4).

The catalysts typically exhibited an initial loss in activity followed by a longer period of slower deactivation (Fig. 4). After an initial stabilization period of around 15–20 h, deactivation was much slower, and after 3 days deactivation had virtually ceased. Selectivity for MeSH generally tended to increase during the experiments, until a steady value was reached (Fig. 5). For each case, MeSH was the dominant product, but other products included CS_2, CO_2, and CO.

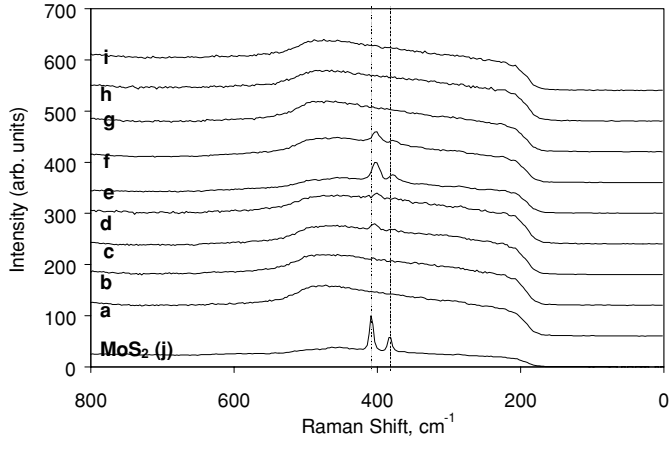

FIG. 3. Laser Raman spectra of the various catalysts examined, after 20 h under reaction conditions (250°C, H_2S/MeOH = 3.00). The bands at 408 and 383 cm^{-1} arise from MoS_2. Letters indicating the various catalysts are as in Table 1.

TABLE 4

Activity and Selectivity Summary for Amorphous Catalysts LaMoS and NaMoS(py) at Various Temperatures and H_2S/MeOH Ratio of 3

	LaMoS			NaMoS(py)		
	250°C	300°C	350°C	250°C	300°C	350°C
BET S.A. (m^2/g) (pre/postreaction)	170/116	170/66	170/55	135/49	135/7.1	135/2.7
Approximate contact time (s)	0.87	0.79	0.73	0.87	0.79	0.73
MeOH conversion						
mol%	8.9	46.3	91.3	4.3	25.0	49.1
$mol/m^2 \cdot s \times 10^8$	0.29	2.6	6.2	0.3	13.0	67.0
Selectivities (mol%)						
Methane	0.1	0.6	6.1	0.3	1.7	1.9
Ethene/acetylene	0.0	0.1	0.4	0.0	0.0	0.0
Ethane	0.0	0.0	0.1	0.0	0.0	0.0
Propane	0.0	0.1	0.2	0.0	0.0	0.0
Dimethylether	0.2	0.0	0.0	0.0	0.0	0.0
Methanethiol	82.5	57.2	53.2	64.3	43.1	40.3
Ethanethiol	0.0	0.2	0.2	0.0	0.1	0.0
Dimethylsulfide	5.4	5.6	5.1	0.4	0.1	0.1
CS_2	5.7	20.4	0.8	0.0	0.1	0.0
CO	2.8	2.0	7.9	8.5	16.7	22.1
CO_2	3.4	13.3	25.4	11.6	29.3	30.4
COS	0.1	0.5	0.5	14.9	9.0	5.2

Note. Data represents the average for the final 5 h of a 72-h run.

Also detected were CH_4, DMS, and trace amounts of DME (Table 4). For LaMoS, as temperature and conversion increased, the selectivity to MeSH dropped significantly, but remained above 50% even at 350°C, where nearly full conversion was attained. At the elevated temperatures, selectivity for CH_4 increased steadily, as did the amount of CO_2 produced. However, the selectivity for CS_2 was highest at 300°C, while the selectivity for CO was lowest. Between 300 and 350°C, amorphous NaMoS(py) had a steady-state selectivity for MeSH of about 40–43%, independent of temperature. For both LaMoS and NaMoS(py), significant differences in selectivity occurred only among CO, CO_2, CS_2, and COS for this temperature range.

N_2 adsorption analysis was performed before and after reaction for LaMoS and NaMoS(py) (Table 4). In all cases, the catalysts underwent significant losses in BET surface area during the reaction, particularly at higher reaction temperatures. Examination of the BJH results for amorphous LaMoS indicated that the decrease of surface area could be attributed to the loss of small pores having diameters of less than about 70 Å (Fig. 6); larger pores were apparently unaffected.

LRS performed on LaMoS and NaMoS(py) before and after reaction at the various temperatures (Fig. 7) clearly showed that MoS_2 was formed during reaction, and that this transformation was more pronounced at above 300°C. Only a slight indication of MoS_2 peaks was observed in the spectra of these catalysts after reaction at 250°C. Additionally, FTIR spectra for the amorphous LaMoS material after reaction clearly showed the formation of MoS_2 for the samples after reaction at temperatures above 300°C (Fig. 8). Again, there was only a very slight indication that MoS_2 was present at 250°C.

Surface analysis of the LaMoS catalysts by XPS before and after reaction for three days at 250, 300, and 350°C showed substantial changes (Fig. 9). Both the Mo 3d peaks and the S 2p peaks shifted to higher binding energies at higher temperatures. Deconvolution of peaks in the Mo 3d region for both LaMoS and NaMoS(py) catalysts (before and after reaction) showed the presence of at least four Mo environments (Table 5). Prior to reaction, the major Mo species detected had the low binding energy characteristic of Mo in the Mo_6S_8 cluster (about 227.3–227.9 eV for the Mo $3d_{5/2}$ peak) (21). A small amount of Mo in a higher oxidation state consistent with MoO_3 (about 231.4–232.9 eV) was also observed in many materials: this was consistent with the formation of MoO_3, likely due to oxygen contamination during the handling procedures.

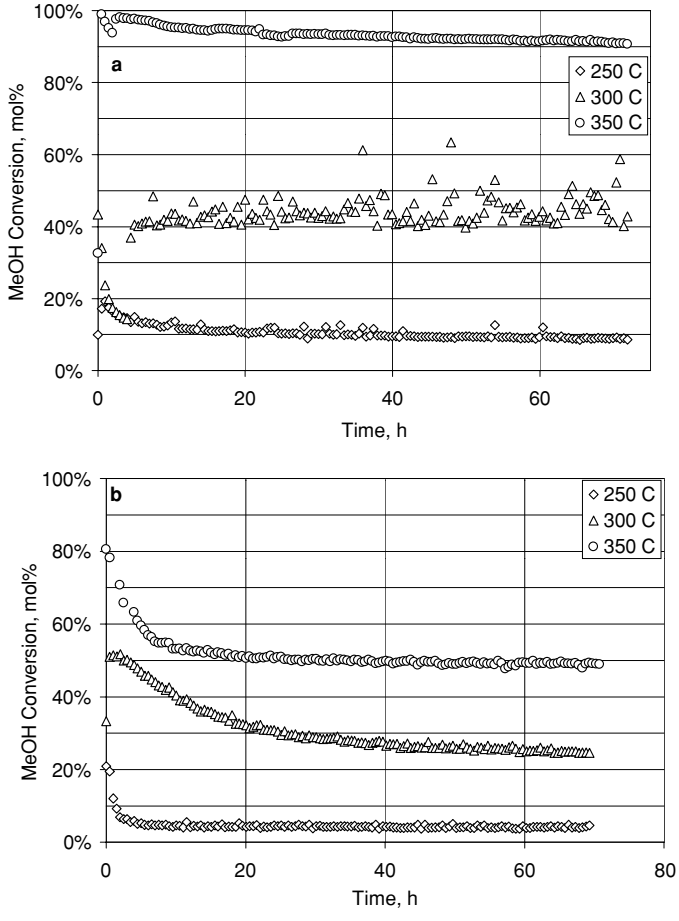

FIG. 4. Conversion for H_2S + MeOH over the amorphous catalysts (a) LaMoS and (b) NaMoS(py) at various temperatures and constant H_2S/MeOH ratio of 3.00.

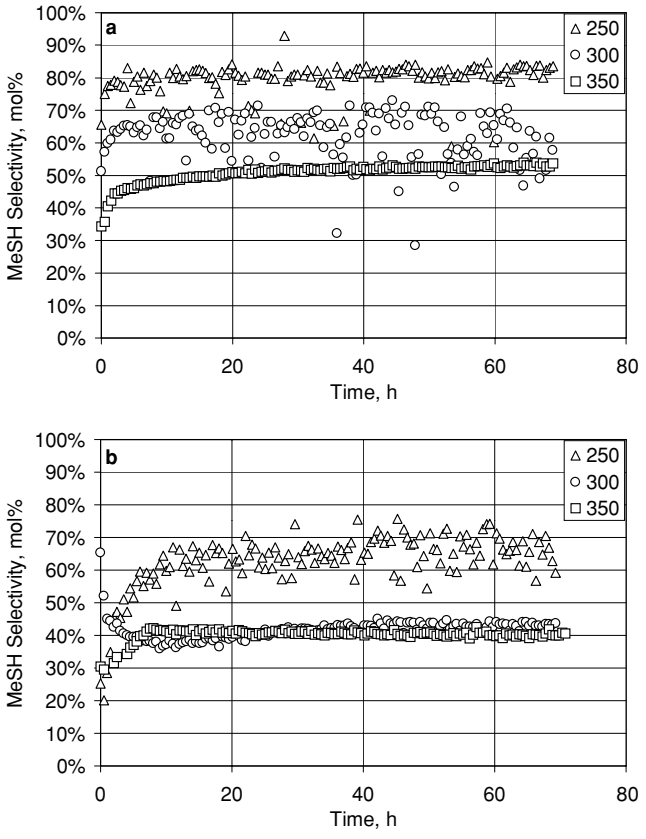

FIG. 5. Selectivity to MeSH for H_2S + MeOH over the amorphous catalysts (a) LaMoS and (b) NaMoS(py) at various temperatures and constant H_2S/MeOH ratio of 3.00.

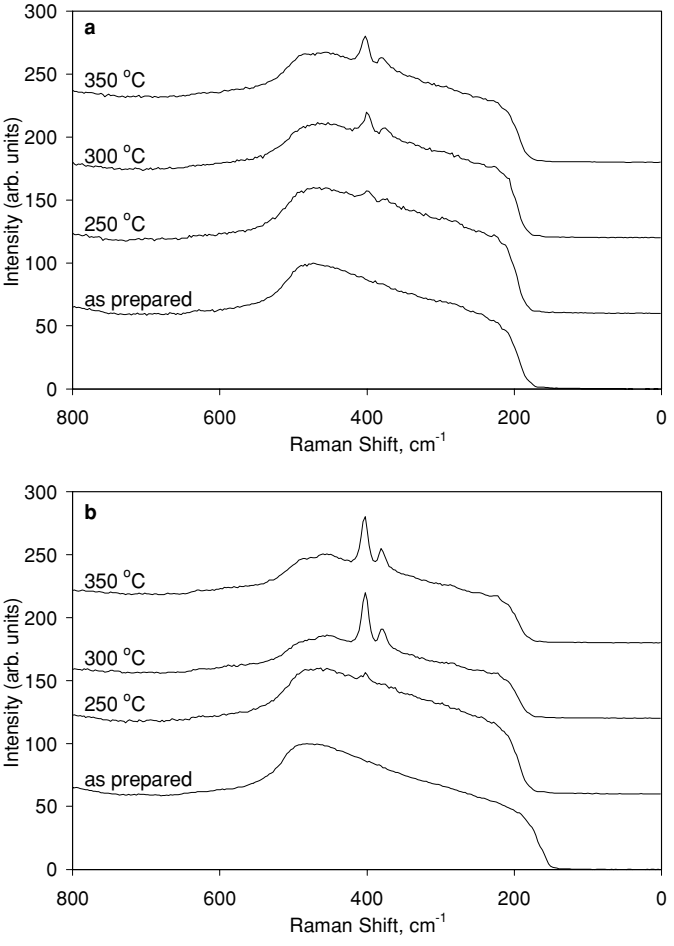

FIG. 7. Laser Raman spectra of amorphous catalysts (a) LaMoS and (b) NaMoS(py) before and after reaction for 3 days at various temperatures and constant H_2S/MeOH ratio of 3.00. Small amounts of MoS_2 were detected, indicated by peaks at about 383 and 404 cm^{-1}.

Following reaction, the catalysts revealed the presence of Mo surface species with intermediate oxidation states, as was observed in our prior HDS studies (22, 23). The intermediate Mo oxidation states were +3 to +4. Specifically,

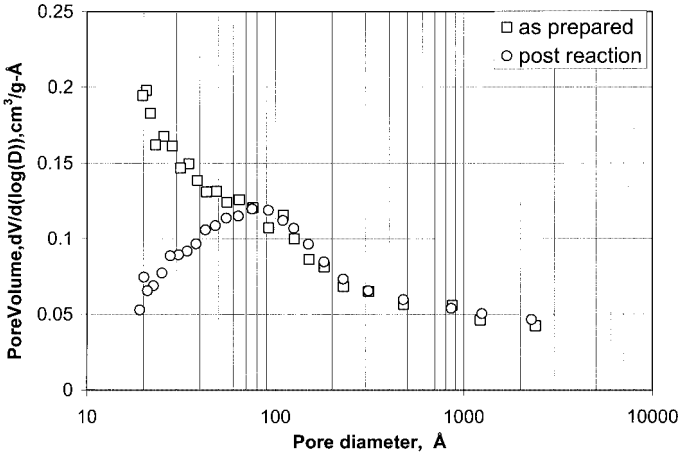

FIG. 6. Porosimetry by nitrogen adsorption at 77 K for amorphous LaMoS, before and after reaction. Reaction causes loss of surface area, resulting from collapse of pores smaller than about 70 Å.

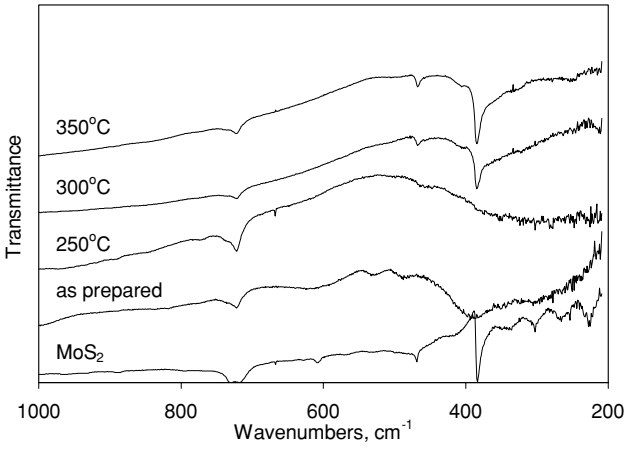

FIG. 8. Fourier transform infrared spectra of amorphous LaMoS before and after reaction for 3 days at various temperatures and constant H_2S/MeOH ratio of 3.00. Peaks at 670 cm^{-1} arise from the mineral oil mulling agent.

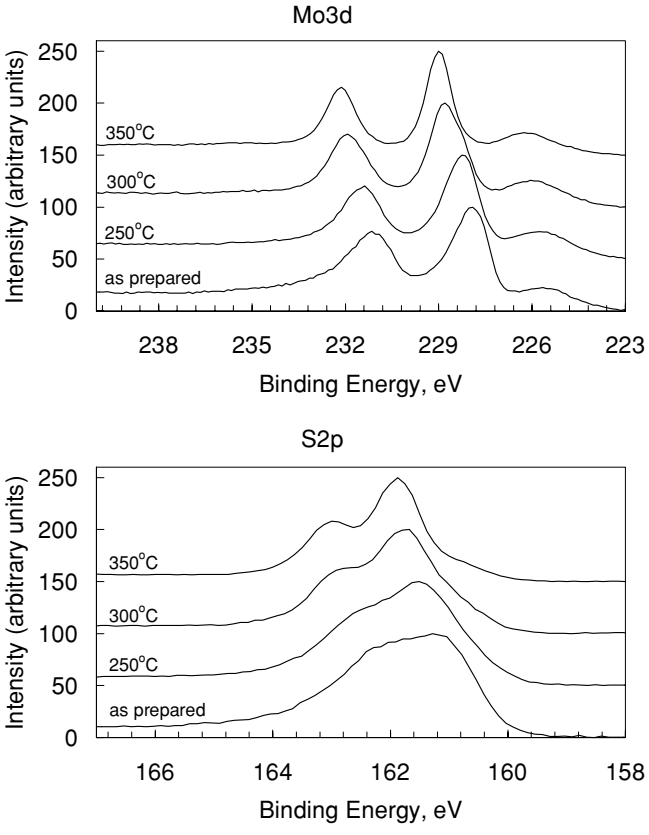

FIG. 9. X-ray photoelectron spectra of amorphous LaMoS catalyst for Mo 3d and S 2p regions, before and after reaction at various temperatures. Reaction conditions caused a shift in the major Mo and S species to higher binding energies, consistent with Mo_2S_3.

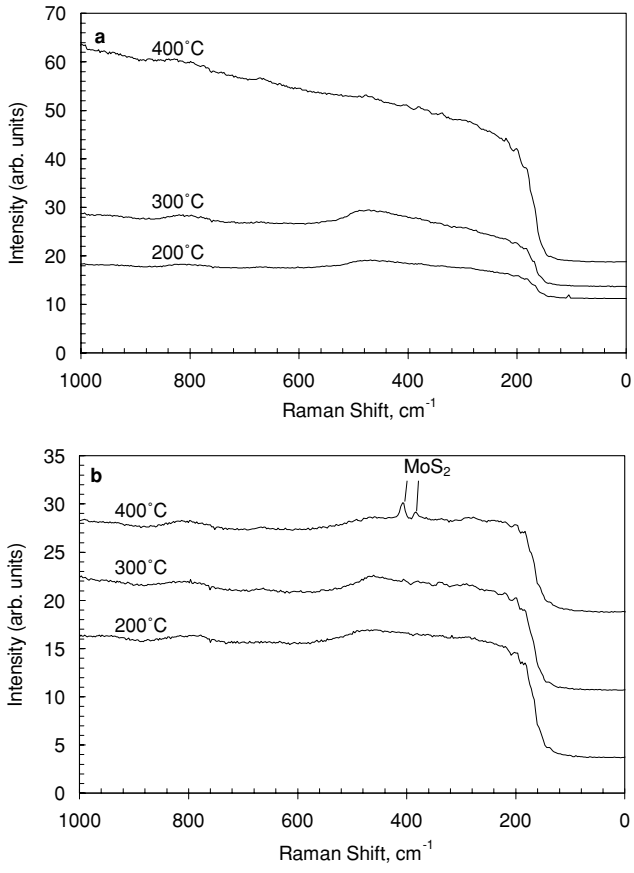

FIG. 10. Laser Raman spectra of amorphous LaMoS after treatment in (a) a stream of MeOH in He and (b) a stream of pure H_2S, at 200, 300, and 400°C for 4 h. Weak bands characteristic of MoS_2 (404, 383 cm^{-1}) are present only in the sample treated in pure H_2S at 400°C. No MoO_3 was detected.

Mo^{3+} was observed at binding energies of 228.4–229.0 eV, consistent with Mo_2S_3 (228.7 eV) (23). Mo^{4+} corresponded to binding energies of 229.5–230.2 eV, consistent with MoS_2 (229.5 eV). After reaction the major species was Mo^{3+}, and the low binding energy characteristic of the cluster was not apparent. Following reaction at 250°C, Mo^{4+} was easily detectable; however after reaction at higher temperatures (300–350°C), this species was apparently converted to Mo^{3+}.

TABLE 5

X-Ray Photoelectron Spectroscopy Summary for the Mo 3d Region of Both Catalysts, before and after Reaction for 3 Days at Various Temperatures and H_2S/MeOH Ratio of 3

	Cluster		Mo^{3+}		Mo^{4+}		Mo^{6+} (MoO_3)	
Catalyst	E_b (eV)	Frac. (%)	E_b (eV)	Frac. (%)	E_b (eV)	Frac. (%)	E_b (eV)	Frac. (%)
LaMoS								
As prepared	227.8	70	228.7	18			231.4	12
Postreaction 250°C			228.4	70	229.5	30		
Postreaction 300°C			228.7	94			231.6	6
Postreaction 350°C			229.0	93			232.1	7
NaMoS(py)								
As prepared	227.3	88	228.4	12				
Postreaction 250°C			228.4	63	229.2	37		
Postreaction 300°C			228.8	100				
Postreaction 350°C			228.8	98	230.2	2		

TABLE 6

X-Ray Photoelectron Spectroscopy Summary for the Mo 3d Region of LaMoS Catalyst, before and after 4-h Treatment with MeOH/He or Pure H_2S at Various Temperatures

Catalyst	Cluster		Mo^{3+}		Mo^{4+}		Mo^{6+} (MoO_3)	
	E_b (eV)	Frac. (%)	E_b (eV)	Frac. (%)	E_b (eV)	Frac. (%)	E_b (eV)	Frac. (%)
As prepared	227.8	70	228.7	18			231.4	12
MeOH treatment temp. (°C)								
200	227.5	34			229.5	66		
300	227.4	40			230.5	50	232.8	10
400	227.7	27			229.5	64	232.9	9
H_2S treatment temp. (°C)								
200	228.1	100						
300			228.5	76	230.0	24		
400			228.8	86	230.2	14		

XPS spectra for the S 2p region of LaMoS catalysts examined after reaction showed a shift to higher binding energies. However, the binding energy of the S $2p_{3/2}$ peak was still a little too low (161.9 eV) to be considered MoS_2 (162.4 eV) (24).

To further elucidate the transformation of amorphous LaMoS to produce intermediate surface oxidation states, studies were performed in the presence of MeOH or H_2S alone. For these studies, LRS and XPS were performed on amorphous LaMoS that was treated either in MeOH in He or in pure H_2S at temperatures ranging from 200 to 400°C for 4 h. For the samples treated with MeOH only (Fig. 10a), no Mo oxides were detected with LRS. LRS of the samples treated in pure H_2S at 400°C (Fig. 10b) revealed no Mo oxides and a small amount of MoS_2 (404 and 383 cm^{-1}). XPS results (Mo $3d_{5/2}$ region) for LaMoS samples treated with only MeOH in He or with only H_2S are summarized in Table 6. After treatment with only MeOH in He at high temperatures, the peak due to the Mo_6S_8 cluster was still present. No conversion to a Mo^{3+} state was detected. However, two higher-oxidation-state surface species were present (binding energies of ~229.4–230.5 and ~232.8) similar to MoO_2 (229.6) and MoO_3 (232.7) (24). In contrast, the Mo 3d regions of the XPS spectra for samples treated in pure H_2S and for samples after MeSH synthesis at similar temperatures showed that the major species was the Mo^{3+}.

DISCUSSION

Activity

All the materials examined in this work seem to be active for MeSH synthesis from MeOH and H_2S. For the amorphous catalysts, the activities initially decreased quickly and then tended to stabilize for an extended time period. This is probably due at least in part to the loss in surface area that the amorphous catalysts experienced. However, specific activity based on catalyst surface areas generally indicated that those catalysts having the lowest surface areas had the highest specific activity on a per-unit surface area basis.

The piperidine-ligated molecular cluster material showed an increase in surface area during reaction. This material at least partially deligated under reaction conditions, as piperidine was detected in the reactor product stream for a few hours after initially reaching 250°C. This is similar to the deligation studies in previous work (25), which indicated that this material deligated at temperatures below 250°C. As the material deligated, the expected tendency would be for it to begin to cross-link at the sites freed up by deligation. If deligation proceeded in a random manner, then rearrangement of clusters upon cross-linking would be rather random as well. Rearrangement of clusters could be expected to continue until three (or more) of the deligated bridging positions on a cluster were linked to another cluster; then the arrangement would be "locked" into place. The resulting arrangement would be less organized than the starting crystalline material and would probably have a slightly higher surface area.

Selectivity

The selectivity of LaMoS catalyst to produce MeSH was maintained even at very low values of H_2S/MeOH ratio. This, combined with the fact that excess H_2S suppressed the overall reaction, implies that H_2S is very strongly adsorbed on amorphous LaMoS. If the partial pressure of H_2S is excessive, the adsorption of MeOH may be inhibited or blocked, thus reducing the overall reaction rate. Lower requirements for H_2S partial pressures may be attractive since the overall safety of the process may be enhanced.

At the start of each reactor run, a relatively high selectivity toward DMS was observed, but this decreased within a few hours to the steady-state value. Related work has indicated that the formation of DMS on metal oxide catalysts requires different types of surface sites (as characterized by their acidity or basicity) compared to MeSH synthesis (26). These sites may deactivate differently, or at least at differing

rates. The initial drop in DMS selectivity could arise if the sites responsible for DMS production were initially deactivated more rapidly than those responsible for MeSH formation.

An alternative explanation for this effect depends on the surface mechanism. If the surface mechanism is similar to that reported by Mashkin (27), it is possible that the initial surface concentration of CH_3O (or CH_3S) is higher than the concentration at steady state, since initially SH is consumed by CH_3O to form CH_3S. Later, the concentration of SH is much higher, preventing the reaction of surface CH_3O or CH_3S with CH_3S to form DMS.

For NaMOS(py) catalysis, increasing conversion by raising temperature led to a significant increase in CO and CO_2 production and to a slight increase in CH_4 production. As previously mentioned, H_2 was also detected in the reactor effluent in small amounts. It is possible that the Mo_6S_8 materials also catalyze additional reactions. The overall stoichiometric conversions that could be considered include the following:

$$CH_3OH \xrightarrow{Mo_6S_8} CO + 2H_2, \quad [5]$$

$$CH_3OH + H_2 \xrightarrow{Mo_6S_8} CH_4 + H_2O, \quad [6]$$

$$CH_3SH + H_2 \xrightarrow{Mo_6S_8} CH_4 + H_2S, \quad [7]$$

$$CO + H_2S \xrightarrow{Mo_6S_8} COS + H_2, \quad [8]$$

$$2COS \xrightarrow{Mo_6S_8} CO_2 + CS_2, \quad [9]$$

$$COS + H_2O \xrightarrow{Mo_6S_8} CO_2 + H_2S. \quad [10]$$

An important property of these catalysts is that the major side product for alumina-based MeSH synthesis catalysts, DMS, was either not present at all or formed in very small amounts. Moreover, certain major side products in this work, CO, CO_2, CS_2, and COS, are not important side products for reactions with alumina-based catalysts.

Stability

MoS_2 was detected by LRS in amorphous ternary materials containing Na, Pt, or Sn after reaction for 20 h with MeOH and H_2S, but not for materials containing La or Ho. Formation of MoS_2 was more apparent for the "small ion" materials, probably due to the mobility and loss of the ternary metal from the surface. Destabilization of the Mo_6S_8 clusters could lead to MoS_2 formation.

A small amount of MoS_2 was also detected for LaMoS by LRS and FTIR after reaction for 3 days. The amount of MoS_2 increased with reaction temperature and was clearly detectable by 300°C. Prior HDS work with this catalyst at higher temperatures (400°C) did not show the presence of any MoS_2 in postreaction characterization. However, for the HDS studies, the partial pressure of H_2S was much lower. In addition, the HDS studies were carried out for only 10 h, and there is a significant difference in the amount of MoS_2 formed at longer reaction times.

XPS analysis of LaMoS and NaMoS(py) revealed interesting changes occurring near the catalyst surface during reaction. By 250°C under reaction conditions with H_2S present, the Mo in the cluster was apparently altered, primarily due to significant conversion to the intermediate Mo^{3+} species and partial conversion to Mo^{4+} (MoS_2). MoS_2 was detected by XPS only at the surface; none was observable by LRS or FTIR. Reaction at higher temperatures (300–350°C) with H_2S present formed only the Mo^{3+} species at the surface. However, in the bulk, the material seems to substantially convert to MoS_2, as shown by the LRS and FTIR results.

Samples treated in only MeOH in He did not show any conversion to the Mo^{3+} species by XPS; rather they revealed significant conversion to an oxysulfide species, with binding energies consistent with Mo^{4+}. The fact that the Mo peak due to the cluster remained present up to 350°C in samples heated in only MeOH (no H_2S present)—combined with the fact that the Mo^{3+} species was not detected in these samples—indicates that the Mo^{3+} species is most likely a purely sulfide species like Mo_2S_3. These results also imply that this Mo^{3+} species does not form by disproportionation of the Mo and S in the Mo_6S_8 cluster; rather it requires the presence of additional sulfur source, such as H_2S.

XPS results showed the presence of Mo^{4+} at the surface for catalyst treated in pure H_2S at 300–400°C. However, the relative amount of Mo^{4+} seemed to decrease with increasing temperature. This fact, combined with the postreaction XPS results, seems to indicate that MoS_2 is not the most surface-stable species on these materials; rather it is a more reduced form with Mo^{3+}, perhaps a material like Mo_2S_3. This is somewhat surprising considering their stoichiometries; in excess H_2S one could expect that MoS_2 would be more stable.

Samples treated in pure H_2S did not reveal bulk conversion to MoS_2 (detected by LRS) until the temperature was above 300°C. However, XPS on postreaction materials showed that the MoS_2 was formed at 250°C and was not present at the surface by 300°C; instead, only the Mo^{3+} species was detected. Under reaction conditions, some surface oxide or oxysulfide formed by oxidation with the alcohol or other oxygen-containing compounds at 250°C, which in the presence of H_2S rapidly converted to MoS_2. However, these studies also have shown that the presence of MeOH is not required to form MoS_2 from LaMoS in the bulk, since a detectable amount formed at 400°C in pure H_2S after only 4 h.

CONCLUSIONS

Amorphous ternary materials based on the Mo_6S_8 cluster represent a new and interesting family of mercaptan

synthesis catalysts due to their low selectivity to DMS and higher selectivity to the unusual side products CO, CO_2, COS, and CS_2. These materials naturally fall into three main categories: amorphous ternary materials, crystalline Chevrel phases, and ligated crystalline molecular cluster materials. The most active, selective, and stable materials for MeSH synthesis were the amorphous ternary materials, where the ternary metal was of the "large ion" type (La, Ho). Though the amorphous LaMoS catalyst did form some MoS_2 after 3 days on stream, this material maintained activity for several days and exhibited MeSH selectivities higher than 80% in the reaction of H_2S with MeOH at 250°C. The ligated crystalline molecular cluster materials had reasonably high activity and were surprisingly stable, even though they did undergo slight deligation at 250°C. The crystalline La Chevrel phase material was also very stable, but had much lower selectivity to MeSH than its amorphous counterpart. The least stable catalysts examined tended to be the "small ion" amorphous ternary materials, which partially converted to MoS_2 under reaction at 250°C in only 20 h.

ACKNOWLEDGMENTS

We thank Jim Anderegg of the Ames Laboratory for assistance in obtaining the XPS characterization. We also thank Shane Hilsenbeck for preparing several of the catalysts used in this work. This work was supported by the U.S. Department of Energy, Office of Basic Energy Sciences, through Ames Laboratory, operated by Iowa State University under Contract W-7405-Eng-82.

REFERENCES

1. Forquy, C., and Arretz, E., *Stud. Surf. Sci. Catal.* **41**, 91 (1988).
2. U.S. Patent 4,233,128 to Societe Nationale Elf-Aquitaine (Production), (1980).
3. U.S. Patent 5,741,934 to S. R. Sandler, P. J. Peerce-Landers, and C. Forquy (1998).
4. U.S. Patent 5,405,820 to Elf Atochem North America, Inc. (1995).
5. U.S. Patent 5,898,012 to Phillips Petroleum Company (1999).
6. U.S. Patent 5,283,369 to Elf Atochem North America, Inc. (1994).
7. European Patent Application 564 706 A1 to Elf Atochem North America, Inc. (1992).
8. U.S. Patent 5,874,630 to Occidental Chemical Corporation (1999).
9. U.S. Patent 5,741,934 to S. R. Sandler, P. J. Peerce-Landers, and C. Forquy (1998).
10. U.S. Patent 4,410,731 to Pennwalt Corp. (1983).
11. Barrault, J., Boulinguiez, M., Forquy, C., and Maurel, R., *Appl. Catal.* **33**, 309 (1987).
12. Hilsenbeck, S. J., Young, V. G., and McCarley, R. E., *Inorg. Chem.* **33**(9), 1822 (1994).
13. Hilsenbeck, S. J., McCarley, R. E., Thompson, R. K., Flanagan, L. C., and Schrader, G. L., *J. Mol. Catal. A* **122**, 13 (1997).
14. McCarty, K. F., and Schrader, G. L., *Ind. Eng. Chem. Prod. Res. Dev.* **23**, 519 (1984).
15. McCarty, K. F., Anderegg, J. W., and Schrader, G. L., *J. Catal.* **93**, 375 (1985).
16. Eckman, M. E., Anderegg, J. W., and Schrader, G. L., *J. Catal.* **117**, 246 (1989).
17. Ackman, R. G., *J. Gas. Chrom.*, June, 1964.
18. Ackman, R. G., *J. Gas. Chrom.*, October, 1968.
19. Chang, C. H., and Chan, S. S., *J. Catal.* **72**(1), 139 (1981).
20. Wieting, T. J., and Verble, J. L., *Phys. Rev. B* **3**(12), 4286 (1971).
21. McCarley, R. E., Hilsenbeck, S. J., and Xie, X., *J. Solid State Chem.* **117**, 269 (1995).
22. Hilsenbeck, S. J., McCarley, R. E., Goldman, A. I., and Schrader, G. L., *Chem. Mater.* **10**, 125 (1998).
23. Thompson, R. K., Hilsenbeck, S. J., Paskach, T. J., McCarley, R. E., and Schrader, G. L., *J. Mol. Catal A* **161**, 75 (2000).
24. Lavasseur, A., Vinatier, P., and Gonbeau, D., *Bull. Mater. Sci.* **22**(3), 607 (1999).
25. Hilsenbeck, S. J., and McCarley, R. E., *Chem. Mater.* **7**, 499 (1995).
26. Mashkina, A. V., *Russ. Chem. Rev.* **64**(12), 1131 (1995).
27. Mashkin, V. Yu., *Appl. Catal. A* **109**, 45 (1994).